Tellus (1999), 51A, 273–288
Printed in UK – all rights reserved

TELLUS
ISSN 0280–6495

Transient moist baroclinic instability

By MICHAEL K. TIPPETT*, *Centro de Previsão de Tempo e Estudos Climáticos, INPE, Brazil*

(Manuscript received 6 March 1998; in final form 29 September 1998)

ABSTRACT

The non-modal transient properties of the Eady baroclinic model with a simple heating parameterization are examined. The time-dependent non-modal behavior of the moist baroclinic model is investigated by calculating the energy amplification of *optimal perturbations* for relevant time-scales and by calculating the energy evolution of random initial conditions. Enhanced non-modal growth on time-scales of 1–2 days is present on all length-scales considered. Exponentially neutral length-scales present algebraic growth which is substantially enhanced in the presence of condensational heating. On time-scales of 1–2 days, maximum growth occurs on shorter length-scales than those predicted by previous normal mode calculations. Heating is found to reduce the time required for uncorrelated random perturbations to organize and grow, though for moderate heating, this time is still relatively long.

1. Introduction

The idealized models of Charney (1947) and Eady (1949) describe how horizontal temperature gradients, and in turn, vertical velocity shear, provide the potential energy for baroclinic instability. Normal mode analysis of these models identifies perturbations that grow exponentially in time. The time and length-scales of these modal instabilities are comparable to observed mid-latitude synoptic-scale cyclones. However, the normal modes (eigenmodes) of these baroclinic models, and of shear flows in general, do not form a complete orthogonal basis, i.e., the linear models are *non-normal* (Held, 1985). A distinguishing feature of non-normal models is that their behavior as given by the *initial value* approach can be quite different than that suggested by normal mode analysis (Farrell and Ioannou, 1996). As a consequence of their non-normality, the Charney (1947) and Eady (1949) baroclinic models present features such as (i) non-modal growth in the absence of exponential instability and (ii) enhanced variance levels in response to stochastic forcing (Farrell, 1989; Farrell and Ioannou, 1993). An understanding of both the modal and non-modal behavior of these baroclinic models is necessary to make fair comparisons between models and observed phenomena. For instance, it has been proposed that the development of type-B cyclones can be explained using a superposition of modally neutral solutions of the Eady model (Farrell, 1985; Rotunno, 1989).

Diabatic processes are another important mechanism in cyclogenesis. Case studies and theoretical models have indicated that including latent heating in cyclogenesis models can lead to faster development and shorter length-scales (Kuo and Reed, 1988; Kristjánsson, 1990). As latent heating processes are complex and occur on time and length scales much shorter than synoptic scales, what actually appears in these models are parameterizations that describe the effect of diabatic processes on the synoptic-scale motions. Two idealized heating parameterization schemes are based on (i) a form of reduced static stability

* Address: Centro de Previsão de Tempo e Estudos Climáticos, Instituto Nacional de Pesquisas Espaciais, Rodovia Presidente Dutra km 40, Cachoeira Paulista, SP 12630-000, Brazil. email: tippett@cptec.inpe.br

(Emanuel et al., 1987) and (ii) Conditional Instability of the Second Kind (CISK, Charney and Eliasson, 1964; Mak, 1982). The behavior of models with parameterizations based on the these approaches has been studied analytically and numerically using normal mode analysis in the context of baroclinic instability (Bonatti and Rao, 1988; Fantini, 1993). Though the non-modal properties of dry baroclinic dynamics are known to be important (Davies and Bishop, 1994; Farrell and Ioannou, 1996), as far as we know, no study has been made of the non-modal properties of moist baroclinic dynamics.

There are several reasons for the preference given to normal mode analysis. Normal mode analysis gives a concise, time-independent (and for models with a complete set of orthogonal eigenmodes, a complete) picture of the behavior of disturbances. In contrast, spatial structures and growth-rates of non-modal behavior are time-dependent. For simple flows and simple geometries, normal mode analysis often provides clear insightful analytical results; in very few cases can non-modal behavior be analyzed without resort to numerical methods. However, the same need for computational methods is present in normal mode analysis of problems with nontrivial flows and geometry. Finally, as has been often stated, normal mode analysis does identify the exponentially growing solutions and all disturbances must evolve into the most unstable normal mode in the limit of long time. However, a priori one does not know either the time-scale on which modal behavior becomes dominant nor the importance of non-modal behavior on intermediate time-scales. Therefore, the value of normal mode analysis is increased when it is accompanied by estimates of its validity.

This paper examines the non-modal properties of the Eady model with Mak's (1982) heating parameterization, a linear parameterization that has been used in various studies (Bonatti and Rao, 1988; Aravequia et al., 1995). A more general heating parameterization was presented in Mak (1994) though for the situation emphasized here, weak to moderate heating, the two schemes are similar. As in studies mentioned previously, a major limitation of this work is its failure to treat the fundamentally non-linear aspects of the problem. Additionally the simplicity of the model means that except for qualitative features the results here are not generally directly applicable to realistic scenarios. Useful quantitative results would require the use of a more sophisticated model.

The paper is organized as follows. In Section 2 we review the moist Eady model and its normal mode analysis. The time-dependent model is presented and two methods are used to investigate its time-dependent non-modal behavior in Section 3. The first, *optimal perturbations*, calculates the maximum possible energy amplification on a given time-scale (Farrell, 1989). Enhanced non-modal growth on time-scales of 1 to 2 days is seen on all length-scales. The relaxation from non-modal to modal behavior depends on the modal stability of the wavelength and is non-uniform in the heating intensity. The 2nd method of analysis considers the time evolution of random initial perturbation. Heating is found to shorten the time required for random perturbations to organize and grow, though the time required for random perturbations to organize is still relatively long. Summary and conclusions are given in Section 4.

2. Moist Eady model

The governing perturbation equations for a two-dimensional Eady model in pressure coordinates are the vorticity equation

$$\left(\frac{\partial}{\partial t}+\bar{u}\frac{\partial}{\partial x}\right)\frac{\partial^2\psi}{\partial x^2}=f\frac{\partial\omega}{\partial p}, \tag{1}$$

and the thermodynamic equation

$$\left(\frac{\partial}{\partial t}+\bar{u}\frac{\partial}{\partial x}\right)\frac{\partial\psi}{\partial p}-\frac{\mathrm{d}\bar{u}}{\mathrm{d}p}\frac{\partial\psi}{\partial x}=-\frac{S}{f}\omega-\frac{RQ}{fp}. \tag{2}$$

The independent variables are the zonal coordinate x, the pressure p and time t. The unknowns are the perturbations stream-function $\psi=\psi(x,p,t)$ and the perturbation vertical velocity $\omega=\omega(x,p,t)$. The condensational heating rate is denoted by Q and f is the Coriolis parameter. The Eady model has a constant static stability S and a basic flow $\bar{u}$ that is linear in the pressure. The horizontal and vertical domains respectively are $0\leqslant x\leqslant L$ and $p_{\mathrm{T}}\leqslant p\leqslant p_{\mathrm{S}}$; L is the horizontal length-scale; p_{S} and p_{T} are respectively the pressure at the surface and at the top of the model. The vertical velocity perturbation ω is assumed to

vanish at the upper and lower pressure boundaries, giving the boundary conditions

$$\omega(x, p, t) = 0, \qquad p = p_S, p_T, \tag{3}$$

The assumption of no heating at the boundaries provides the boundary conditions

$$\left(\frac{\partial}{\partial t} + \bar{u}\frac{\partial}{\partial x}\right)\frac{\partial \psi}{\partial p} - \frac{d\bar{u}}{dp}\frac{\partial \psi}{\partial x} = 0,$$

$$p = p_S, \quad p = p_T. \tag{4}$$

Eqs. (1) and (2) can be used to derive the omega equation

$$\frac{\partial^2 \omega}{\partial p^2} + \frac{S}{f^2}\frac{\partial^2 \omega}{\partial x^2} = \frac{2}{f}\frac{d\bar{u}}{dp}\frac{\partial^3 \psi}{\partial x^3} - \frac{\partial^2}{\partial x^2}\left(\frac{RQ}{fp}\right), \tag{5}$$

and the potential vorticity equation

$$\left(\frac{\partial}{\partial t} + \bar{u}\frac{\partial}{\partial x}\right)\left(\frac{S}{f^2}\frac{\partial^2 \psi}{\partial x^2} + \frac{\partial^2 \psi}{\partial p^2}\right) = -\frac{\partial}{\partial p}\left(\frac{RQ}{fp}\right). \tag{6}$$

Eqs. (5) and (6) along with the boundary conditions (3) and (4) form the set of equations that will be investigated.

The system of eqs. (5) and (6) has been analyzed using normal mode analysis (Mak, 1982; Bonatti and Rao, 1988). In normal mode analysis the unknowns are assumed to be periodic in x with period L and the x and t dependence of the perturbations ψ and ω has the form

$$\omega(x, p, t) = \tilde{\psi}(p)\exp[i(kx - \gamma t)], \tag{7}$$

and

$$\chi(x, z, t) = \bar{\omega}(p)\exp[i(kx - \gamma t)], \tag{8}$$

where the wavenumber k is related to the length-scale by $k = 2\pi/L$. Substituting (7) and (8) into (5) and (6) gives 2 equations for $\tilde{\omega}$ and $\tilde{\psi}$

$$\Delta\tilde{\omega} = -\frac{2}{f}\frac{d\bar{u}}{dp}ik^3\tilde{\psi} + k^2\frac{R\tilde{Q}}{fp}, \tag{9}$$

and

$$-i(\gamma - \bar{u}k)\Delta\tilde{\psi} = -\frac{\partial}{\partial p}\left(\frac{R\tilde{Q}}{fp}\right), \tag{10}$$

where the linear operator Δ is defined by

$$\Delta \equiv \frac{\partial^2}{\partial p^2} - \frac{S}{f^2}k^2, \tag{11}$$

and $\tilde{Q}$ is the Fourier component of the heating rate Q, as yet unspecified. The boundary conditions for (9) and (10) follow directly from those in (3) and (4).

The heating parameterization suggested by Mak (1982) is to take the heating rate to be related to the dynamically induced vertical velocity $\tilde{\omega}_a$, that is, the vertical velocity obtained from (5) without the heating term. In this parameterization the condensational heating is proportional to the dynamically induced cloud-base vertical velocity W_b multiplied by a prescribed heating profile $\hat{h}(p)$ and a nondimensional heating intensity parameter ε. The heating profile is prescribed, though a dynamically regulated profile would be more realistic. Explicitly, the heating rate is

$$\tilde{Q}(k, p) = -\varepsilon\hat{h}(p)\tilde{W}_b(k), \tag{12}$$

where $\tilde{W}_b(k) = \Pi_b\{\tilde{\omega}_a(k, p)\}$, Π_b is the linear operator defined by

$$\Pi_b\{g(k, p)\} = g(k, p_b); \tag{13}$$

p_b is the cloud-base pressure. Using (9) without the heating term as the equation for $\tilde{\omega}_a$ gives the expression for $\tilde{Q}$ in terms of $\tilde{\psi}$ as

$$\tilde{Q} = \frac{2ik^3}{f}\varepsilon h(p)\frac{d\bar{u}}{dp}\Pi_b\Delta^{-1}\tilde{\psi}; \tag{14}$$

the inverse of the operator Δ is uniquely defined using the boundary condition from (3). Having written the heating rate $\tilde{Q}$ as a linear function of $\tilde{\psi}$, (10) can be written as an eigenvalue problem

$$(-i\gamma\mathbf{I} - \mathbf{A})\tilde{\psi} = 0 \tag{15}$$

where the linear operator $\mathbf{A}$ is given by

$$\mathbf{A} = \mathbf{A}(k, \varepsilon)$$

$$\equiv \Delta^{-1}\left(-ik\bar{u}\Delta - \varepsilon\frac{2ik^3}{f}\frac{dh}{dp}\frac{d\bar{u}}{dp}\Pi_b\Delta^{-1}\right), \tag{16}$$

and the normalized heating profile $h(p)$ is given by $h(p) = \hat{h}(p)/p$; $\mathbf{I}$ is the identity operator. The boundary condition (4) is used to uniquely define (16). Eq. (15) has a non-zero solution when $(-i\gamma\mathbf{I} - \mathbf{A})$ is singular, that is when $-i\gamma$ is an eigenvalue of $\mathbf{A}$.

The properties of the eigenvalues of $\mathbf{A}$ determine the existence of exponentially growing instabilities. Suppose that c_0 is an eigenvalue of $\mathbf{A}$ and that $\tilde{\psi}_0(p)$ is the associated eigenfunction; $\mathbf{A}\tilde{\psi}_0 = c_0\tilde{\psi}_0$. The corresponding perturbation stream-function ψ is given by

$$\psi(x, p, t) = \tilde{\psi}_0(p)\exp[ikx + c_0 t]. \tag{17}$$

If the real part of the eigenvalue c_0 is greater than zero then there are exponentially growing eigenmodes. The maximal exponential (or modal) growth rate β is defined by

$$\beta = \max_{z \in \Lambda(\mathbf{A})} \mathrm{Re}\, z, \tag{18}$$

where $\Lambda(\mathbf{A})$ denotes the set of eigenvalues of $\mathbf{A}$. Mak (1982) used the normalized heating profile $h(p)$ given by

$$h(p) = \begin{cases} 1, & 400\ \mathrm{mb} \leqslant p \leqslant 900\ \mathrm{mb} \\ 0, & p < 400\ \mathrm{mb}\ \text{or}\ p > 900\ \mathrm{mb}, \end{cases} \tag{19}$$

and obtained analytical expressions for the modal growth rate β which were used to determine the dependence of β on the wavenumber k and the heating parameter ε. In Fig. 1 for the heating profile of (19) the modal growth rate β is shown as a function of the wavelength L for several values of ε; a surface pressure $p_S = 1000$ mb and upper boundary pressure $p_T = 150$ mb were used and $\bar{u} = 30/(p_T - p_S)$; $S = 0.04\ \mathrm{m^2\ s^{-2}\ mb^{-2}}$; length-scales L between 5×10^5 m and 5×10^7 m were considered. Two significant features of Fig. 1 are that for the larger values of the heating parameter ε, the exponential growth rate increases and the length-scale L associated with the maximum modal growth rate decreases, physically reasonable behavior. The values of the heating parameter ε used correspond to physical values that are not unreasonable (Mak, 1982).

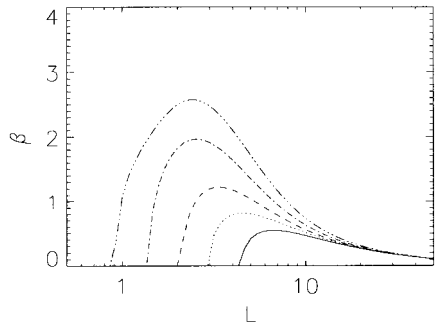

Fig. 1. Eigenvalue analysis of **A**. The modal growth rate β in units of $10^{-5}\ \mathrm{s^{-1}}$ as a function of the wavelength L in units of 10^6 m for $\varepsilon = 0.0$ (solid), 0.2 (dotted), 0.4 (dashed), 0.8 (dash dot), 1.5 (dash-dot-dot-dot).

The dependence of the growth rate and length-scale on the heating is made more clear in Figs. 2a and 2b where the maximum (with respect to L) modal growth rate and its associated wavelength are shown as functions of the heating parameter ε. For this range of values of the heating parameter ε there is a minimum wavelength at which exponential instability is possible and a maximum (with respect to ε) growth rate. As discussed in Mak (1982) the existence of growth rate saturation and decline as the heating rate is increased is a fundamental difference between the usual wave-CISK parameterization and that used here. The maximal exponential growth rate of the dry Eady model is about $5.5 \times 10^{-6}\ \mathrm{s^{-1}}$ with length-scale of about 6.65×10^6 m. With the addition of the Mak (1982) heating parameterization with $\varepsilon = 1.6$, the maximum exponential growth rate is about $2.7 \times 10^{-5}\ \mathrm{s^{-1}}$ with a length-scale L of about 2.7×10^6 m, a considerable increase in growth rate and decrease in length-scale.

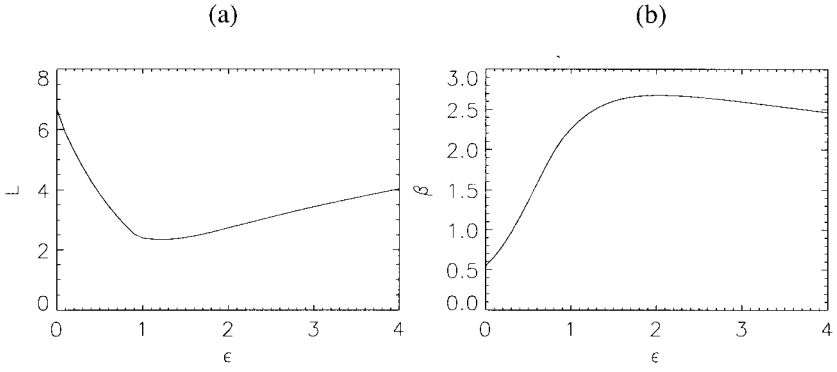

Fig. 2. Eigenvalue analysis of **A**. Panel (a) the wavelength L in units of 10^6 m of the most unstable eigenmode as a function of the heating parameter ε. Panel (b) as (a) but for the maximal growth rate β.

The data shown in Figs. 1, 2, equivalent to that obtained using the analytical formulation of Mak (1982), was obtained using a quasi-geostrophic finite-difference multilevel model (Bonatti and Rao, 1988). A finite-difference model with 40 vertical levels is used to construct the matrix $\mathbf{A}$. Test calculations with 100 vertical levels presented no significant differences. The values shown in Fig. 1 were obtained by computing the eigenvalues of $\mathbf{A}$ for a particular L and ε and then calculating the modal growth rate β. The maximal growth rates and corresponding length-scales shown in Fig. 2 were found by solving an optimization problem for each value of ε; the range of length-scales L was restricted to be $5 \times 10^5\ \mathrm{m} \leqslant L \leqslant 5 \times 10^7\ \mathrm{m}$. For this range of parameters, there is at most one unstable eigenmode. Though not shown here, the numerical results support the conjecture (Mak, 1982) that there is an additional continuous spectrum as is seen in the dry Eady model and in other moist baroclinic models (Bannon, 1986).

3. Time-dependent behavior

The eigenvalue analysis of the moist baroclinic model presented in Section 2 can also be interpreted in terms of a time-dependent problem. The time-dependent formulation follows from defining the perturbation stream-function ψ and the perturbation vertical velocity ω in terms of the time-dependent variables ω' and ψ' given by

$$\psi(x, p, t) = \psi'(p, t) \exp(ikx), \tag{20}$$

and

$$\omega(x, z, t) = \omega'(p, t) \exp(ikx). \tag{21}$$

In contrast to (7) and (8) the time evolution of the perturbations is not constrained to be exponential. Then, noting that formally $\partial/\partial t = -i\gamma$, it follows from (15) that the time evolution of the time-dependent perturbation stream-function ψ' is given by the differential equation

$$\frac{\partial \psi'}{\partial t} = \mathbf{A}\psi'; \tag{22}$$

$\mathbf{A}$ is defined in (16). The solution of (22) with initial condition $\psi'(p, t=0) = \psi'_0(p)$ is

$$\psi'(p, t) = \mathrm{e}^{t\mathbf{A}}\psi'_0(p). \tag{23}$$

The exponential of a matrix can be defined, for example, in terms of a power series (Golub and Vand Loan, 1996, Subsection 11.3). This explicit representation of the solution is used to investigate the properties of the time-dependent system in what follows.

3.1. Optimal perturbations

A useful measure of the time-dependent behavior of a perturbation with initial value ψ'_0 is the ratio of perturbation energy at time t to initial perturbation energy

$$\frac{\|\psi'(p, t)\|^2}{\|\psi'_0\|^2}, \tag{24}$$

where the energy norm $\|\cdot\|$ is defined for any function $g(k, p)$ as the sum of the kinetic and available potential energy

$$\|g(k, p)\|^2 = \frac{1}{2}\langle k^2 g^2 \rangle + \frac{f_0^2}{2}\left\langle \frac{1}{S}\left(\frac{\partial g}{\partial p}\right)^2 \right\rangle; \tag{25}$$

$\langle\cdot\rangle$ denotes average over the domain. Other norms may be of interest. For example, to study a dry Eady model Davies and Biship (1994) used the thermal and pressure growth rates as measures of the perturbation behavior. Associated with the norm in (25) is an inner product. The energy norm on perturbations induces a norm on the operator $\mathrm{e}^{t\mathbf{A}}$ defined by

$$\|\mathrm{e}^{t\mathbf{A}}\| = \max_{\|\psi'_0\| \neq 0} \frac{\|\psi'(p, t)\|}{\|\psi'_0\|}. \tag{26}$$

Therefore $\|\mathrm{e}^{t\mathbf{A}}\|^2$ is the maximum factor by which the perturbation energy can be amplified in t time units. Details of the energy norm calculations are given in Section 6. In Farrell (1989) the initial perturbation ψ'_0 that produces this maximum growth is referred to as a finite-time *optimal perturbation.*

If the eigenfunctions of the operator $\mathbf{A}$ are orthogonal with respect to the inner product associated with the norm $\|\cdot\|$, then the connection between the time-dependent behavior of the perturbation energy and the eigenvalue analysis is strong. In particular, a direct calculation shows that the maximal perturbation energy growth is modal and

$$\|\mathrm{e}^{t\mathbf{A}}\| = \mathrm{e}^{\beta t}, \tag{27}$$

where β is the modal growth rate defined in eq. (18). In this case, the optimal perturbation that

produces the maximum growth at time t is independent of t and is the eigenfunction of $\mathbf{A}$ whose eigenvalue has real part β. However, if the eigenvectors of $\mathbf{A}$ are not orthogonal and complete (equivalently if $\mathbf{A}$ is non-normal), then the maximum energy growth is generally not modal; that is, the optimal perturbations are generally not eigenfunctions of $\mathbf{A}$ and the maximum amplification of the optimal perturbations is generally greater than the modal growth rate. Additionally, the optimal perturbation generally depends on the optimization time. As the optimal perturbation evolves in time its structure and partitioning of kinetic and potential energy change.

The normal mode analysis does give information even when the eigenvectors of $\mathbf{A}$ are not orthogonal. First, the maximum energy amplification is always at least as large as that predicted by normal mode analysis

$$\| e^{t\mathbf{A}} \| \geqslant e^{\beta t}. \tag{28}$$

Therefore, the growth rates shown in Fig. 1 are lower bounds for the non-modal growth. To compare the modal and non-modal growth rates it is convenient to define a time-dependent energy growth rate $\alpha(t)$ by

$$\alpha(t) = \frac{1}{t} \ln \| e^{t\mathbf{A}} \|. \tag{29}$$

When $\mathbf{A}$ is normal, $\alpha(t)$ is equal to the constant β. In general, only in the limit of large-time does the energy growth rate $\alpha(t)$ coincide with the modal growth rate β. Precisely, the following limit must be satisfied (Halmos, 1967, Problem 74)

$$\lim_{t\to\infty} \alpha(t) = \beta. \tag{30}$$

However, the time required for the energy growth rate $\alpha(t)$ to be well approximated by the modal growth rate β is problem dependent. Examples may be constructed where this time is arbitrarily long (Trefethen, 1997). Therefore, as stated in the Introduction a principle aim of this work is to identify the time-scale on which the energy growth rates and structures are those given by normal mode analysis and to examine the behavior of the model on intermediate time-scales.

The quantity $\alpha(0)$, called the numerical abscissa of $\mathbf{A}$, is related to the maximum possible rate of change of the energy as shown by

$$\begin{aligned}\alpha(0) &= \left[\frac{1}{\tau} \max_{\|\psi(t)\| \neq 0} \ln \frac{\|\psi(t+\tau)\|}{\|\psi(t)\|} \right]_{\tau=0} \\ &= \left[\max_{\|\psi(t)\| \neq 0} \frac{\ln \|\psi(t+\tau)\| - \ln \|\psi(t)\|}{\tau} \right]_{\tau=0} \\ &= \max_{\|\psi(t)\| \neq 0} \frac{\mathrm{d}}{\mathrm{d}t} \ln \|\psi(t)\|. \end{aligned} \tag{31}$$

If $\mathbf{A}$ is normal, it can be diagonalized by an orthogonal transformation and $\alpha(0) = \beta$. However, Fig. 3 shows that here the behavior of the maximum rate of change of the energy $\alpha(0)$ is quite different from the modal growth rate β shown in Fig. 1. The quantity $\alpha(0)$ is, like β, larger for the larger values of the heating parameter ε. However, the maximal energy growth rates are substantially greater than the exponential growth rates. Additionally in all the cases the maximum energy growth rate is either achieved or nearly achieved at the lower bound of the range of length-scales considered, $L = 5 \times 10^5$ m. This amplification of energy at short horizontal length-scales may well have numerical stability consequences in nonlinear simulations where there is coupling between different horizontal wave numbers.

The weak dependence of $\alpha(0)$ on the length-scale in the dry model was previously noted by Farrell and Ioannou (1996). In that work it was shown that $\alpha(0)$ has its maximum at short length-scales and that only on very long wavelengths ($k \to 0$) does $\alpha(0)$ go to zero. Somewhat different behavior was seen in Davies and Bishop (1994) where the perturbations of the dry Eady model were formulated in terms of two edge waves

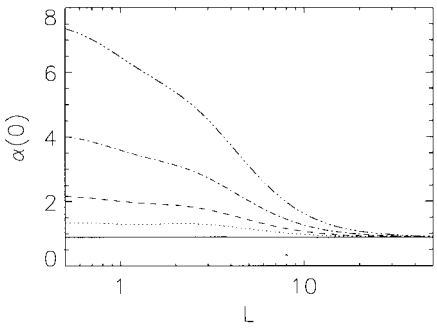

Fig. 3. As in Fig. 1 but for the maximum rate of change of the energy $\alpha(0)$.

propagating on the upper and lower boundaries. The maximum thermal and pressure growth rates were found to be larger than the normal mode growth rates with the maximum pressure growth rates being associated with short length-scales and the maximum thermal growth rates with *long* length-scales.

The physical relevance of this behavior depends on what time-scale the maximum energy growth rate $\alpha(0)$ can be maintained before relaxing to the modal growth rate β (see eq. (30)). In Fig. 4 the energy growth rate $\alpha(t)$ is shown as a function of the length-scale L for $t = 12$ h, 24 h, 48 h and 5 days. A striking feature is that for these time-scales there is no clear length-scale cut-off as is seen in Fig. 1, indicating that the wavelengths with zero modal growth rate present substantial (compared to the dry or weak heating cases) non-modal growth even on periods as long as 5 days. The limit (30) indicates that for long enough time, the energy growth rates must go to zero for wavelengths where there are no exponentially growing modes. However, the limit (30) is a rather weak constraint on possible growth in the exponentially stable case. When $\beta = 0$, algebraic growth $\sim t^{\eta}$ for any power η is not precluded. After five days the energy growth-rates of these exponentially stable waves is not very close to zero. In fact, the 48-h energy growth rate of exponentially stable wavelengths is little less than that of the modal growth rates associated with exponentially unstable wavelengths for the dry or nearly dry (small ε) Eady model; all are on the order of $10^{-5}\ \mathrm{s}^{-1}$.

More insight to this behavior is obtained by examining the energy growth rate $\alpha(t)$ and the operator norm $\|e^{t\mathbf{A}}\|$ as functions of time for exponentially stable wave-lengths. In Fig. 5 the energy growth rate and operator norm are shown as functions of time for $L = 750$ km, a exponentially stable length-scale. For large values of the heating parameter ε there is considerable transient growth that is reflected in a large initial growth rate. During an initial phase the growth rate

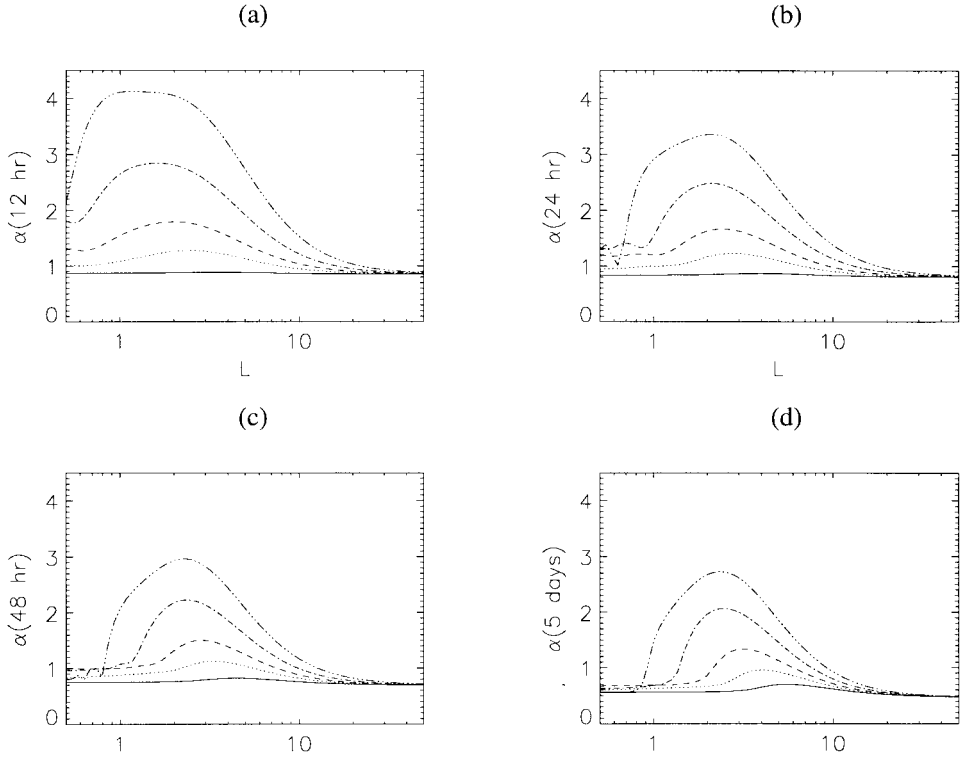

Fig. 4. As in Fig. 3 but the energy growth rate $\alpha(t)$ for (a) $t = 12$ h, (b) $t = 24$ h, (c) $t = 48$ h and (d) $t = 5$ days.

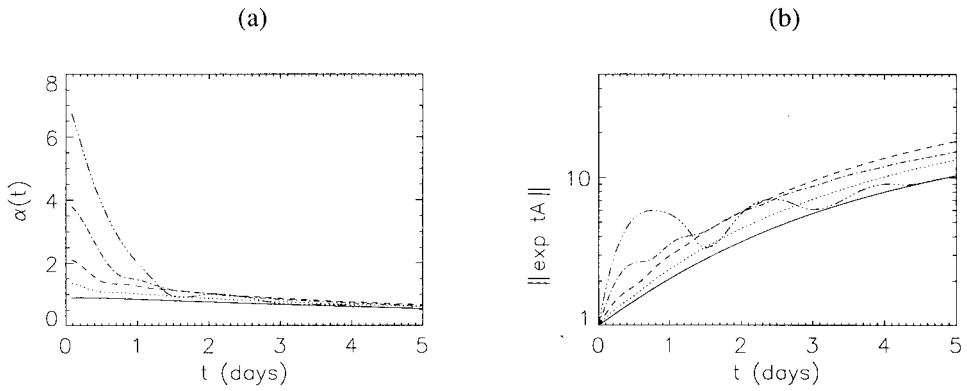

Fig. 5. For the modally stable length-scale $L = 750$ km the (a) energy growth rate $\alpha(t)$ and (b) the operator norm $\|e^{t\mathbf{A}}\|$ plotted as functions of time for the values of ε and line styles used in Fig. 1.

decays rapidly. This initial phase is about 1.5 days for $\varepsilon = 1.5$; for smaller values of the heating parameter, the initial phase is shorter. After the initial phase, the growth rates decay extremely slowly to zero with little dependence on the value of ε. Fig. 5b shows that the slow decay of the growth rate to zero is due to the persistent, though sub-exponential, growth of the operator norm $\|e^{t\mathbf{A}}\|$; the growth is roughly $\sim t^{1.4}$ for these time-scales. Interestingly, for $\varepsilon = 1.5$ the growth of the operator norm is non-monotonic in time, a feature particular to non-modal behavior. Recall that if the eigenvectors of $\mathbf{A}$ were orthogonal, all the values shown in Fig. 5a would be identically zero and all those in Fig. 5b would be identically unity.

Returning to Fig. 4, it appears that the energy growth rates of length-scales associated with exponentially unstable modes relax more rapidly to their modal growth rates than those associated with modally stable length-scales. This indication is confirmed in Fig. 6 analogous to Fig. 5 but for the length-scales corresponding to the dominant modal instability. The energy growth rates are close to their asymptotic modal values quite quickly. There is some dependence on the heating parameter; for $\varepsilon = 1.5$ there is a short transient phase and then a rapid relaxation to the modal growth rate. For smaller values of ε there is little or no transient phase and a slower relaxation to the modal growth rate. Comparing the growth rates shown in Figs. 5, 6 shows that on time-scales of 1–2 days the energy growth rate of exponentially stable modes may be comparable to that of exponentially unstable modes.

For intermediate modally unstable length-scales, i.e., ones between the short-wave modal

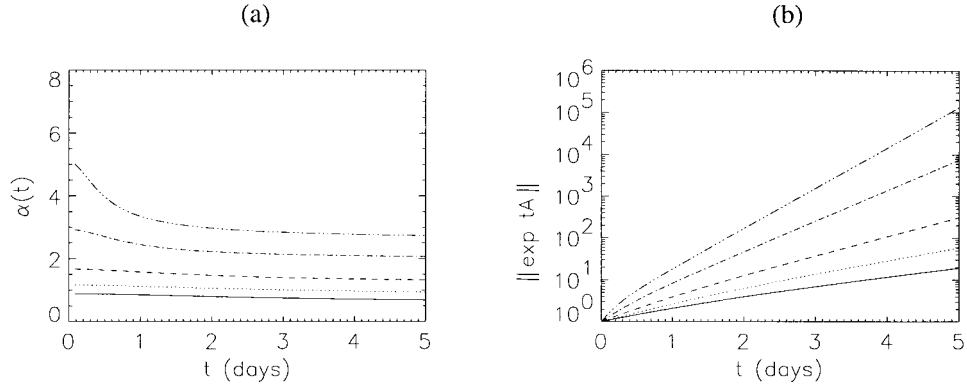

Fig. 6. As in Fig. 5 but for each ε the length-scale is the one with the largest exponential growth rate.

growth rate cut-off and the length-scale at which maximum modal growth occurs, calculations present a mixture of modal and non-modal growth. Modal growth is preceded by non-modal growth which as indicated by the values of $\alpha(0)$ in Fig. 3 is larger than that seen at the length-scale with maximal modal growth. This initial enhanced non-modal growth combining with subsequent modal growth gives maximum growth that is as large or larger than that seen in Fig. 6.

The dependence of the energy growth rates and length-scales on the heating parameter ε for the various time-scales is shown in Fig. 7. Fig. 7a shows the length-scale at which maximum growth occurs as a function of ε. For moderate to intense heating ($\varepsilon > 0.4$), the maximum initial energy growth ($\alpha(0)$) occurs at $L = 500$ km, the smallest length-scale considered. As the energy growth rate $\alpha(t)$ is calculated on longer time-scales, the resulting length-scale curves go from the maximum initial growth rate curve to the normal mode growth rate curve. The discontinuity seen in the 12-h curve is due to the maximum growth rate being achieved at two length-scales. The dependence of the convergence to the normal mode result on ε is clear; for ε small, the convergence is slow; the 48-h maximum energy growth rate for the dry Eady model occurs at a length-scale considerably less than that at which the maximum modal growth rate is seen. For values of ε roughly greater than unity, the 24-h and 48-h curves are quite close to the normal mode analysis curve. Fig. 7b shows the maximum (with respect to L) finite-time growth rates $\alpha(t)$ as a function of ε for several values of t. For small values of ε the non-modal growth rates are slightly higher than the modal growth rate. For larger values of ε the initial maximum growth rate $\alpha(0)$ is approximately linear in ε; though not visible on scale of Fig. 7b, the linearity of $\alpha(0)$ in ε is present also for larger values of the heating parameter. The maximum growth rate $\alpha(0)$ unlike the modal growth rate β does not exhibit saturation as the heating rate increases. The modal growth rate saturation was previously explained as being the result of weakening of the interaction between the potential vorticity (PV) anomalies at the modal boundaries due to the addition of the PV anomalies in the top and bottom of the heating layer (Mak, 1994). However, it would appear that on transient time-scales efficient interaction between the model boundary PV anomalies and the those of the heating layer can occur and lead to growth associated with short horizontal scales. Such growth is not maintained. However, the trend that non-modal growth is larger for large values of ε is seen on fairly long time-scale. At about 48 h, the maximal non-modal growth rate is close to the maximum modal growth rate for all values of ε.

The vertical structure of the optimal perturbations depends on the optimization time. The vertical structure of the optimal perturbation changes as it evolves in time, unlike that of an eigenmode. A key part of the time evolution is the development of interior diabatically generated PV (see eq. (6)). The vertical structure of the dominant eigenmode along with that of the optimal perturbations is shown in Fig. 8. The optimal perturbations have

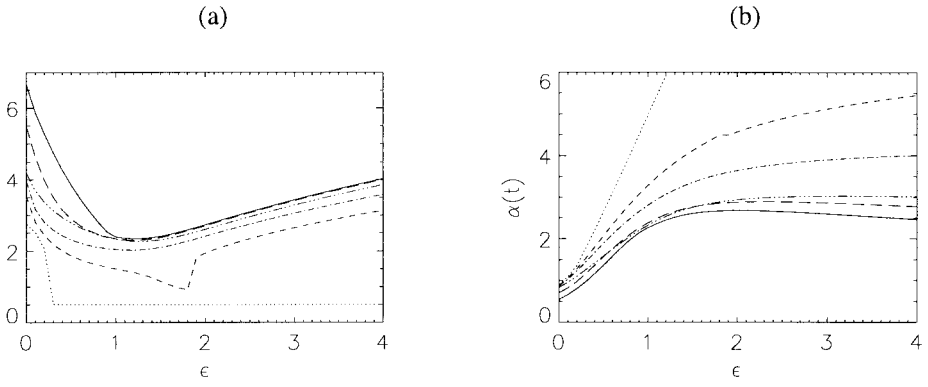

Fig. 7. As in Fig. 2 but for the normal (solid line), initial (dotted line), 12-h (dashed line), 24-h (dashed dotted line), 48-h (dash-dot-dot-dot) and 5-day (long dash) energy growth rates.

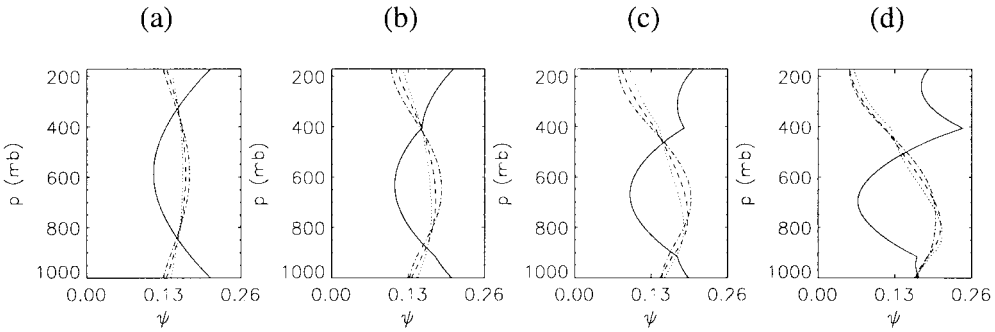

Fig. 8. Vertical structure $|\psi(t)|$ ($\|\psi(t)\|$ normalized to unity) for initial perturbation of the dominant eigenmode (solid) and optimal perturbations for $t = 12$ h (dotted) $t = 24$ h (dashed) and $t = 48$ h (dash dot). The heating parameter ε is (a) 0.0, (b) 0.2, (c) 0.4, (d) 0.8. The length-scale for each ε is the one associated with the fastest growing modal instability.

structures that are quite different from that of the eigenmode. In the limit of large optimization time, the optimal perturbation is the leading eigenmode of the adjoint of **A**. The optimal perturbations are shown at their optimization time in Fig. 9. (In the language of singular vectors, right singular vectors of $e^{t\mathbf{A}}$ appear in Fig. 8 and left singular vectors in Fig. 9.) Though the optimal perturbations have a structure initially quite different from the eigenmode, at their optimization time their structure is not too different from the eigenmode; the similarity is greater for larger values of the heating parameter. The structure of the eigenmodes reflects the PV anomaly sheets located in the top and bottom of the heating layers (Mak, 1994).

Figs. 10, 11 are analogous to Figs. 8 and 9 but show the vertical structure of the optimal perturbations for the exponentially stable length-scale $L = 750$ km. The including of heating has a significant effect on the vertical structure of the modally stable but transiently growing modes. Without heating most of the initial structure is confined to the model boundaries where there are PV anomalies. Addition of heating and the associated PV anomalies at the heating layer boundaries has a strong effect on the regions between the model and heating layer boundaries, initial particularly between the lower model and heating layer boundaries. The evolution in time of the optimal perturbations is less dramatically non-modal than that for modally unstable length-scales with most of the changes in structure occurring at the upper levels.

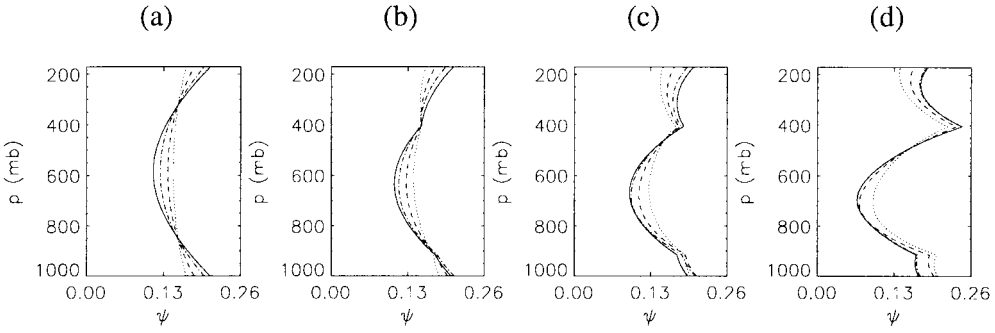

Fig. 9. As in Fig. 8 but at the optimization time.

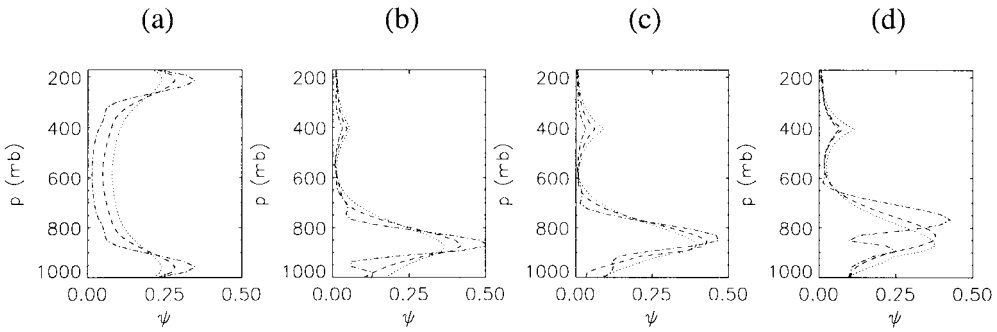

Fig. 10. For the stable length-scale $L = 750$ km the vertical structure $|\psi(t)|$ for initial perturbation of optimal perturbations for $t = 12$ h (dotted), $t = 24$ h (dashed) and $t = 48$ h (dash dot). The heating parameter ε is (a) 0.0, (b) 0.2, (c) 0.4, (d) 0.8.

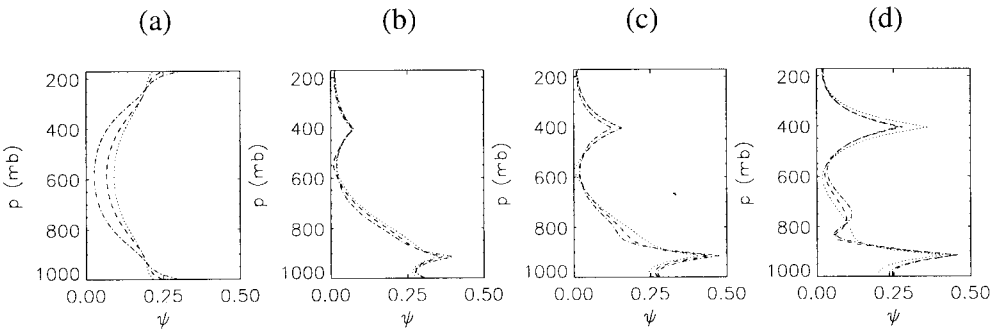

Fig. 11. As in Fig. 10 but at the optimization time.

3.2. *Random initial conditions*

The analysis in the previous subsection examined the energy growth of optimal perturbations, showing that they produce growth greater than the normal modes. In this subsection the growth of *randomly* chosen initial perturbations is investigated. The behavior of randomly chosen initial perturbations gives, in some sense, an idea of the robustness of the optimal perturbations. The general result is that random perturbations are slow to organize and grow, though heating does lead to more rapid development. This result supports the idea that the development of many baroclinic disturbances is explained by the linear growth of initial disturbances with some particularly favorable structure but suggests that strong diabatic processes can make the development considerably less sensitive to the details of the initial conditions.

For a linear problem, quantities such as the energy averaged over random initial conditions can be calculated directly, without need of Monte Carlo simulation. Briefly, the approach is the following. Suppose that the initial value of the perturbation ψ_0' is a mean-zero Gaussian random variable with covariance $\mathbf{C}$; that is

$$E[\psi_0'] = 0, \qquad E[\psi_0'(\psi_0')^*] = \mathbf{C}, \tag{32}$$

where $E[\cdot]$ denotes the expectation operator. The expected energy at time t can be used to define the expected energy growth rate $\rho(t)$ by

$$\rho(t) = \frac{1}{t} \ln E[\,\|\psi'(t)\|\,]. \tag{33}$$

Details of this calculation and of the choice of $\mathbf{C}$ are given in Section 6. Here we use an ensemble of random initial conditions that are homogeneous and uncorrelated (with respect to the energy inner product). A consequence of this choice of $\mathbf{C}$ is that the "most likely" modes are the same as those obtained using optimal perturbations. That is to

say, the left singular vectors of $e^{\tau \mathbf{A}}$ calculated in the preceding Section are the modes that contain the most variance.

Fig. 12, analogous to Fig. 3, shows $\rho(t)$ for various times and values of ε. For times up to 48 h, the magnitude of the growth rate $\rho(t)$ is less than $\alpha(t)$ for both stable and unstable wavelengths. The explanation for this behavior is that random uncorrelated initial conditions, unlike either optimal perturbations or eigenmodes, may require time to organize and grow (Toth and Kalnay, 1997). The behavior seen here is not generic. That is, there is no fundamental reason why the expected energy of random initial conditions cannot grow faster than the leading eigenmode. If the non-modal instability is, in some sense, a broad-spectrum phenomena, then the expected energy growth rate $\rho(t)$ will be greater than the normal mode growth rate β but less than the energy growth rate $\alpha(t)$ (Camargo et al., 1998). Therefore the calculations suggest that the instabilities are not broad-spectrum (in the vertical).

After 5 days $\rho(t)$, like $\alpha(t)$, is fairly close to the modal growth rate β though $\alpha(t)$ is converging to β from above while $\rho(t)$ is converging to β from below. It is important to remember that though the *growth rate* of the ensemble approaches the normal modal growth rate, the average *growth* of the ensemble is substantially less than that of an eigenmode which is in turn less than that of an optimal perturbation (compare Figs. 6, 15). As was also seen with optimal perturbations, there is a tendency for energy amplification at short horizontal wavelengths that is particularly pronounced for small values of ε and short times. This feature is confirmed in Fig. 13a which shows that for small ε and short times, the most unstable wavelength (with respect to the growth rate $\rho(t)$) is $L = 500$ km, the shortest length-scale considered in the model. Discontinuities in the most unstable

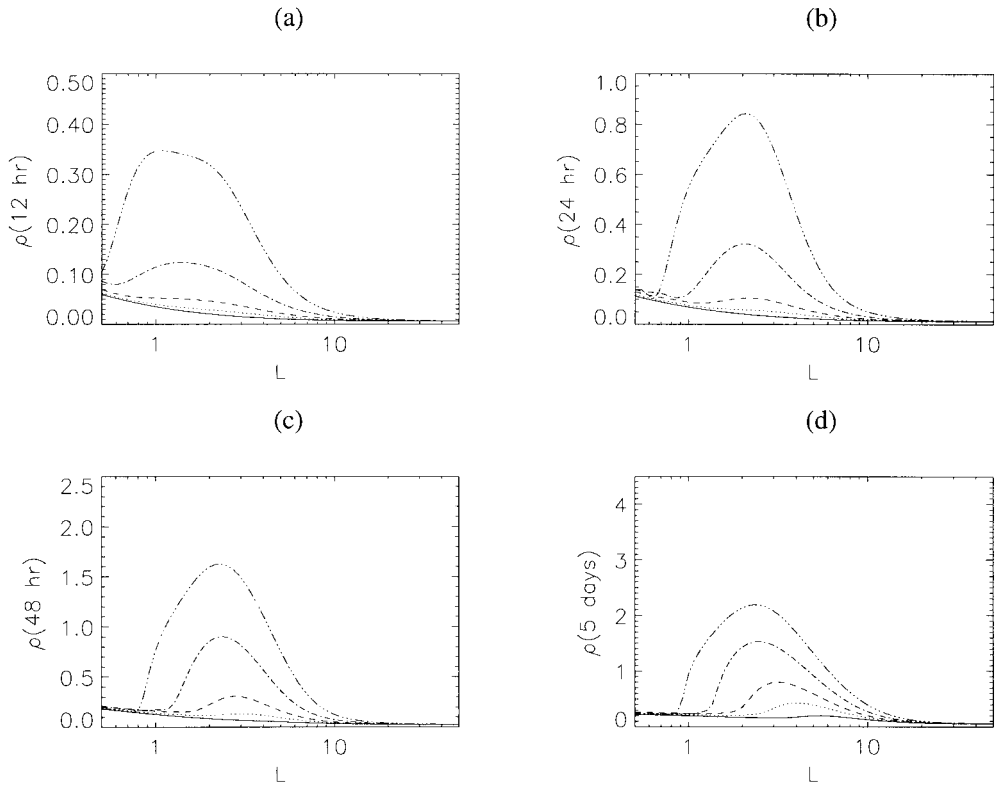

Fig. 12. As in Fig. 3, but the expected energy growth rate $\rho(t)$ for (a) $t = 12$ h, (b) $t = 24$ h, (c) $t = 48$ h and (d) $t = 5$ days.

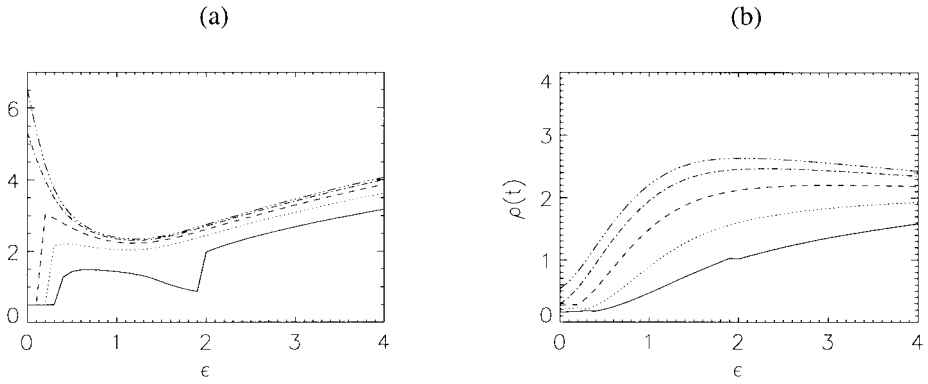

Fig. 13. As in Fig. 2 but the normal (dash-dot-dot-dot) and the expected energy growth rate $\rho(t)$ for $t = 12$ h (solid), $t = 24$ h (dotted), $t = 48$ h (dashed) and $t = 5$ days (dash-dot).

wavelength as a function of ε occur when the maximum growth rate is achieved at two length-scales in the interval $500\text{ km} \leqslant L \leqslant 50\,000$ km. It is reasonable to imagine that the short wavelength amplification not predicted by normal mode analysis would be important in non-linear simulations. Fig. 13b shows the convergence of expected energy growth rate $\rho(t)$ to the modal growth rate β.

Figs. 14, 15 analogous to Figs. 5, 6 show details of the time evolution of the expected energy and its rate of change for exponentially stable and unstable wave numbers respectively. For moderate values of the heating intensity ($\varepsilon \leqslant 0.8$), the addition of heating has little effect on the expected energy evolution of exponentially stable length-scales. For the case of strong heating, $\varepsilon = 1.5$, there is a short-lived transient. For the exponentially unstable wavelengths, increasing the heating parameter increases the eventual modal growth rate and decreases the time for that growth rate to be obtained. Except for large ε, there is little growth for either the stable or unstable length-scales for the time-scales of about a day or two; for small ε the growth of the exponentially stable wavelengths is slightly greater than that of the exponentially stable wavelengths.

4. Summary and conclusions

The finite-time behavior of the baroclinic Eady model with Mak (1982) heating parameterization has been investigated. In this parameterization the heating is related to vertical velocity at the cloud base and a prescribed heating profile; the intensity is controlled by the heating parameter ε. The transient behavior of this moist Eady model, like

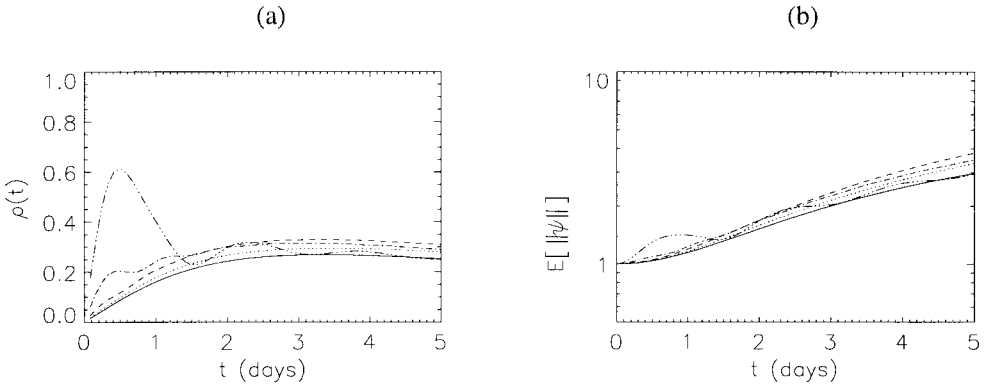

Fig. 14. As in Fig. 5 but for (a) the expected energy $E[\|\psi'(t)\|]$ and (b) the expected energy growth rate $\rho(t)$.

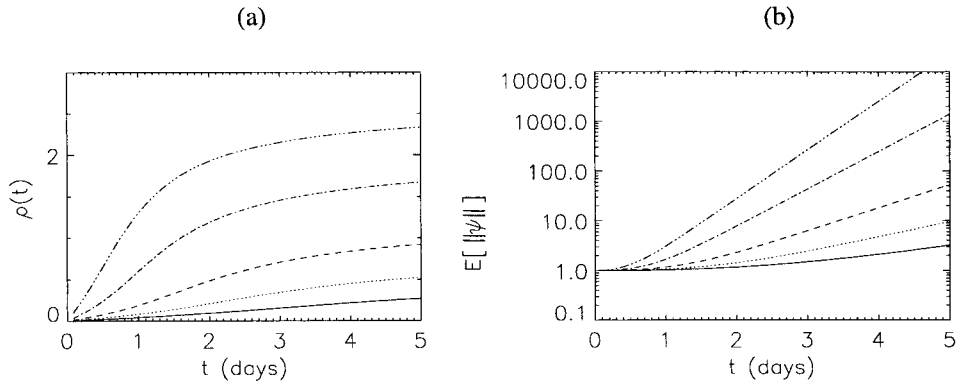

Fig. 15. As in Fig. 6 but for (a) the expected energy $E[\|\psi'(t)\|]$ and (b) the expected energy growth rate $\rho(t)$.

that of the dry Eady model, is richer than suggested by its normal mode analysis. The response of the system to optimal perturbations (optimal in the sense of finite-time growth; Farrell, 1989) and the ensemble-averaged (over random initial conditions) energy evolution were calculated. The main results of the calculations with optimal perturbations are the following.

- The maximum short-time non-modal growth rate is substantially larger than the normal mode growth rate and is an approximately linear, increasing function of the heating intensity. The relaxation of the non-modal growth rate to the normal mode growth rate is non-uniform in the heating intensity.
- Moderate to strong heating produces significant non-modal growth on time-scales up to 24 h.
- For weak to moderate values of the heating intensity, the maximum growth on time-scales of 1–2 days occurs at shorter horizontal length-scales than those predicted by the normal mode analysis.
- On time-scales up to 5 days there is no wavelength cut-off. Algebraic growth of exponentially stable modes results in finite-time growth rates comparable to modal growth rates.
- Heating causes exponentially stable modes to present strong transient growth before showing roughly the same algebraic growth as the dry Eady model.

The main results of the ensemble-averaged calculations are the following.

- The tendency of maximum growth to occur at shorter length-scales than those predicted by normal mode analysis is again seen. For small times ($t \leqslant 24$ h) and small values of the heating parameter ($\varepsilon \leqslant 0.2$), the maximum finite-time growth occurs at the shortest length-scale of the model, 500 km.
- As was seen for the optimal perturbations, only the short-time behavior of exponentially stable wavenumbers is sensitive to the heating intensity; strong heating leads to short-lived transient growth.
- Even for exponentially unstable wavenumbers, random initial conditions take 1–2 days to organize and grow modally; the organization time decreases as the heating parameter increases.

A consequence of this last point is that while strong heating can make rapid development more likely to occur regardless of the details of the initial disturbance, initial disturbances with structure resembling the optimal perturbation grow much faster.

The dependence of moist baroclinic development on initial conditions has consequences for studies that compare the length and time scales of observed phenomena with those given by normal mode analysis (Bonatti and Rao, 1988; Aravequia et al., 1995). As latent heating would appear to play a strong role on the early development of disturbances, a non-modal investigation of moist baroclinic instability is appropriate. Information about non-modal linear behavior is also useful to understand non-linear simulations where often features not predicted by normal mode analysis are attributed to non-linearity alone.

5. Acknowledgments

This work was supported by the Conselho Nacional de Desenvolvimento Científico e

Tecnológico (CNPq) Grant 381737/97-73. Discussions with Drs. Pedro Leite da Silva Dias, Suzana Camargo and Dan Marchesin were highly useful to this study. Thanks are extended to the anonymous reviewers for their careful reading and critical comments.

6. Appendix

For computational purposes it is useful to write the energy norm $\|\cdot\|$ in terms of the usual root mean square norm $\|\cdot\|_2$. For the discrete problem where g_1 and g_2 are vectors, the inner product defined by (25) can be written in the form

$$(g_1, g_2) = g_1^* \mathbf{M}^* \mathbf{M} g_1, \tag{34}$$

where $\mathbf{M}^*\mathbf{M}$ is the definite matrix coming from the discretization of the operators in (25). Then it follows that

$$\|g\|^2 = g^* \mathbf{M}^* \mathbf{M} g = \|\mathbf{M} g\|_2^2, \tag{35}$$

where $\|\cdot\|_2$ is the usual 2-norm. Likewise the energy norm of a matrix $\mathbf{B}$ can be written in terms of the usual matrix 2-norm:

$$\begin{aligned}\|\mathbf{B}\|^2 &= \max_g \frac{\|\mathbf{B} g\|^2}{\|g\|^2} \\ &= \max_g \frac{g^* \mathbf{B}^* \mathbf{M}^* \mathbf{M} \mathbf{B} g}{g^* \mathbf{M}^* \mathbf{M} g} \\ &= \max_f \frac{f^* (\mathbf{M}^{-1})^* \mathbf{B}^* \mathbf{M}^* \mathbf{M} \mathbf{B} \mathbf{M}^{-1} f}{f^* f} \\ &= \|\mathbf{M} \mathbf{B} \mathbf{M}^{-1}\|_2^2,\end{aligned} \tag{36}$$

where $f = \mathbf{M} g$.

The maximum rate of change of the energy $\alpha(0)$ for a given length-scale is obtained by noting that the perturbation energy satisfies the equation:

$$\begin{aligned}\frac{\mathrm{d}}{\mathrm{d}t}\|\psi'\|^2 &= \frac{\mathrm{d}}{\mathrm{d}t}(\psi^* \mathbf{M}^* \mathbf{M} \psi) \\ &= \psi^* (\mathbf{A}^* \mathbf{M}^* \mathbf{M} + \mathbf{M}^* \mathbf{M} \mathbf{A}) \psi.\end{aligned} \tag{37}$$

Therefore

$$\begin{aligned}\alpha(0) &= \max_\psi \frac{\mathrm{d}}{\mathrm{d}t}\|\psi\| = \frac{1}{2}\|\mathbf{A}^* \mathbf{M}^* \mathbf{M} + \mathbf{M}^* \mathbf{M} \mathbf{A}\|_2 \\ &= \frac{1}{2}\|(\mathbf{M} \mathbf{A} \mathbf{M}^{-1})^* + \mathbf{M} \mathbf{A} \mathbf{M}^{-1}\|.\end{aligned} \tag{38}$$

Then an optimization procedure can be used to find the length-scale on which $\alpha(0)$ is largest.

The energy averaged over random initial conditions can be calculated as follows.

$$\begin{aligned}E[(\psi'(t), \psi'(t)] &= E[(\mathrm{e}^{t\mathbf{A}} \psi_0')^* \mathbf{M}^* \mathbf{M}\, \mathrm{e}^{t\mathbf{A}} \psi_0'] \\ &= \mathrm{tr}(\mathbf{M}\, \mathrm{e}^{t\mathbf{A}} E[\psi_0' (\psi_0')^*]\, \mathrm{e}^{t\mathbf{A}^*} \mathbf{M}^*) \\ &= \mathrm{tr}(\mathbf{M}\, \mathrm{e}^{t\mathbf{A}} \mathbf{C}\, \mathrm{e}^{t\mathbf{A}^*} \mathbf{M}^*),\end{aligned} \tag{39}$$

where the initial covariance $\mathbf{C}$ is defined by

$$\mathbf{C} = E[\psi_0' (\psi_0')^*]. \tag{40}$$

It is convenient to take $\mathbf{C} = (\mathbf{M}^*\mathbf{M})^{-1}/n$; the factor of $1/n$ normalizes the expected initial energy to unity. Then

$$E[(\psi'(t), \psi'(t))] = \frac{1}{n}\|\mathbf{M}\, \mathrm{e}^{t\mathbf{A}} \mathbf{M}^{-1}\|_{\mathrm{F}}^2, \tag{41}$$

where $\|\cdot\|_{\mathrm{F}}$ is the usual Frobenius norm. With this choice of initial covariance, the most "likely" vectors in the sense of containing the most variance at time t, are the left singular vectors of $\mathrm{e}^{t\mathbf{A}}$ with respect to the energy inner product. Note that the expected energy $E[\|\psi'(t)\|]$ is always less than or equal to optimal perturbation energy $\|\mathrm{e}^{t\mathbf{A}}\|$ (Golub and Van Loan, 1996, eq. 2.3.7).

REFERENCES

Aravequia, J., Rao, V. B. and Bonatti, J. 1995. The role of moist baroclinic instability in the growth and structure of monsoon depressions. *J. Atmos. Sci.* **52**, 4393–4409.

Bannon, P. R. 1986. Linear development of quasi-geostrophic baroclinic disturbances with condensational heating. *J. Atmos. Sci.* **43**, 2261–2274.

Bonatti, J. P. and Rao, V. B. 1988. Moist baroclinic instability in the development of North Pacific and South American intermediate-scale disturbances. *J. Atmos. Sci.* **44**, 2657–2667.

Camargo, S. J., Tippett, M. K. and Caldas, I. L. 1998. Nonmodal energetics of resistive drift-waves. *Phys. Rev. E* **58**, 3693–3704.

Charney, J. and Eliassen, A. 1964. On the growth of the hurricane depression. *J. Atmos. Sci.* **21**, 68–75.

Charney, J. G. 1947. The dynamics of long waves in a baroclinic westerly current. *J. Meteor.* **4**, 135–162.

Davies, H. C. and Bishop, C. H. 1994. Eady edge waves and rapid development. *J. Atmos. Sci.* **51**, 1930–1946.

Eady, E. T. 1949. Long waves and cyclone waves. *Tellus* **1**, 33–52.

Emanuel, K., Fantini, M. and Thorpe, A. 1987. Baroclinic instability in an environment of small stability to slantwise moist convection. Part I: Two-dimensional models. *J. Atmos. Sci.* **44**, 1559–1573.

Fantini, M. 1993. A numerical study of two-dimensional moist baroclinic instability. *J. Atmos. Sci.* **50**, 1199–1210.

Farrell, B. F. 1985. Transient growth of damped baroclinic waves. *J. Atmos. Sci.* **42**, 2718–2727.

Farrell, B. F. 1989. Optimal excitation of baroclinic waves. *J. Atmos. Sci.* **46**, 1193–1206.

Farrell, B. F. and Ioannou, P. 1996. Generalized stability theory. Part I: Autonomous operators. *J. Atmos. Sci.* **53**, 2025–2040.

Farrell, B. F. and Ioannou, P. J. 1993. Stochastic dynamics of baroclinic waves. *J. Atmos. Sci.* **50**, 4044–4057.

Golub, G. H. and Van Loan, C. F. 1996. *Matrix computations*, 3rd edition. The Johns Hopkins University Press, Baltimore, 694 pp.

Halmos, P. R. 1967. *A Hilbert space problem book*. Van Nostrand-Reinhold, New York, 365 pp.

Held, I. 1985. Pseudomomentum and the orthogonality of modes in shear flows. *J. Atmos. Sci.* **42**, 2280–2288.

Kristjánsson, J. E. 1990. Model simulations of an intense meso-β scale cyclone. The role of condensation parameterization. *Tellus* **42A**, 78–91.

Kuo, Y.-H. and Reed, R. J. 1988. Numerical simulation of an explosively deepening cyclone in the Eastern Pacific. *Mon. Wea. Rev.* **116**, 2081–2105.

Mak, M. 1982. On moist quasi-geostrophic baroclinic instability. *J. Atmos. Sci.* **39**, 2028–2037.

Mak, M. 1994. Cyclogenesis in a conditionally unstable moist baroclinic atmosphere. *Tellus* **46A**, 14–33.

Rotunno, R. and Fantini, M. 1989. Petterssen's "Type B" cyclogenesis in terms of discrete, neutral Eady modes. *J. Atmos. Sci.* **46**, 3605–3610.

Toth, Z. and Kalnay, E. 1997. Ensemble forecasting at NCEP and the breeding method. *Mon. Wea. Rev.* **125**, 3297–3319.

Trefethen, L. N. 1997. Pseudospectra of linear operators. *SIAM Review* **39**, 383–406.